

# PREDICTION OF CRACK INITIATION IN SINGLE CRYSTAL Ni-BASE SUPERALLOYS AT HIGH TEMPERATURES

L.G. Zhao, S. Dumoulin, N. P. O'Dowd and E.P. Busso  
Department of Mechanical Engineering, Imperial College London, UK SW7 2AZ

## ABSTRACT

Because of their excellent high temperature characteristics, Ni-based single-crystal alloys are used in applications where operating temperatures exceed 900°C. The initiation of cracks under these conditions is generally associated with micro-scale porosities (typically between 10 and 20  $\mu\text{m}$ ). These porosities or voids give rise to local intensification of the deformation, leading to microcracking and subsequent failure when adjacent microcracks coalesce and link with a free surface. In this work the initiation of a crack in the vicinity of a relatively blunt notch is examined. Two approaches are adopted—in one approach a void adjacent to the notch is modelled explicitly, in the other a damage variable is used to represent the growth and subsequent cracking of voids in the vicinity of the notch. A finite element approach is adopted in both studies, with a rate dependent slip-system based constitutive law used to represent the mechanical behaviour of the nickel alloy. The effect of oxidation on the predicted initiation times is also discussed.

## 1 INTRODUCTION

A major cause of failure in nickel single crystal alloys operating at high temperatures is the generation of surface cracks. Following initiation, such cracks can grow under thermo-mechanical loading, leading to a loss of integrity of the component. The deformation in the single crystal alloy is anisotropic and controlled by plastic deformation on favourable slip systems. At the relevant temperatures, the operating slip systems for the alloy under consideration, CMSX4, are the cubic ( $\{100\}\langle 011\rangle$ ) slip systems in addition to the octahedral ( $\{111\}\langle 011\rangle$ ) systems. Observation of fracture surfaces in these materials on specimens loaded in the  $\langle 001\rangle$  direction have indicated that fracture occurs by the propagation of microcracks on  $\{001\}$  planes, which appear to have initiated from casting porosities [1]. This fracture mechanism is illustrated in Figure 1.

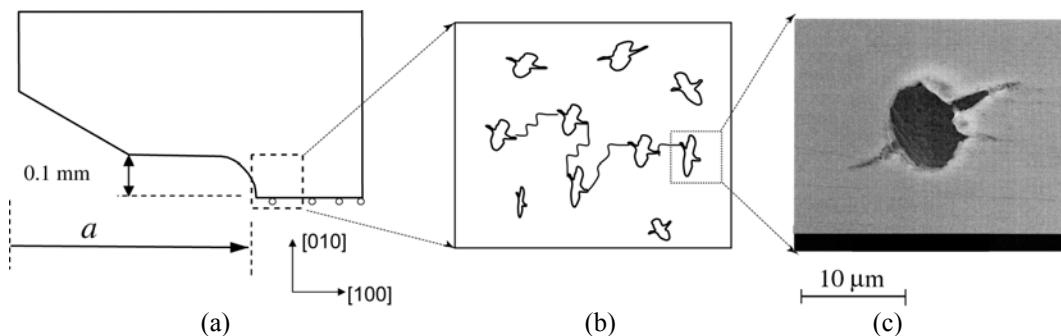


Figure 1: Mechanism of crack initiation in a Ni superalloy, [1] (a) stress/strain concentration at a sharp notch (b) cracking of voids followed by coalescence of microcracks (c) Micrograph of a fracture surface for CMSX4 (from [2])

The porosities in Figure 1 can be considered to exist at the meso-scale, between the macro-scale set by the component dimension (mm) and the micro-scale set by the material microstructure (in this case the size of the second phase  $\gamma'$  precipitates in the CMSX4 alloy, which are between 0.5 and 1  $\mu\text{m}$ ). In this work, two approaches have been examined to represent this fracture

mechanism. An uncoupled damage variable has been incorporated into the material model, which accounts for the growth and subsequent cracking of the voids at the mesoscale. An alternative approach has also been examined where a single void at a fixed distance from the crack tip has been modelled. In the former case fracture initiation is considered to occur when the damage has reached unity at a distance of 50  $\mu\text{m}$  ahead of the notch and in the latter the fracture initiation time is determined as the time when a microcrack first initiates in the vicinity of the notch. The initiation of a microcrack is assumed to be controlled by the attainment of a critical strain in the vicinity of the void.

## 2 MATERIAL CONSTITUTIVE MODEL

The macroscopic stress-strain behaviour of CMSX4 is described by a finite deformation, rate dependent formulation, [2]. Elastic deformation has cubic symmetry, and the inelastic deformation is determined by the accumulation of slip on the relevant CMSX4 slip systems. Thus, the inelastic strain rate,  $\mathbf{L}^p$ , is determined as

$$\mathbf{L}^p = \sum_{\alpha=1}^n \dot{\gamma}^{\alpha} (\mathbf{m}^{\alpha} \otimes \mathbf{n}^{\alpha}), \quad (1)$$

where  $\dot{\gamma}^{\alpha}$  is the strain rate on the slip system  $\alpha$  and  $\mathbf{m}^{\alpha}$  and  $\mathbf{n}^{\alpha}$  are the slip direction and slip plane normal, respectively. Further details of the kinematics of the large strain formulation used in the constitutive model are provided in [1] and [2].

The flow rule for the shear strain rate on a slip system is determined using a stress dependent activation energy, with two internal variables per slip system,  $S$  and  $B$  (see [3]). The inelastic strain rate on a slip system  $\alpha$ , is given by,

$$\dot{\gamma}^{\alpha} = \dot{\gamma}_0 \exp \left[ -\frac{Q_0}{kT} \left( 1 - \left( \frac{|\tau^{\alpha} - B^{\alpha}| - S^{\alpha} \mu / \mu_0}{\tau_0 \mu / \mu_0} \right)^p \right)^q \right] \text{sgn}(\tau^{\alpha} - B^{\alpha}), \quad (2)$$

where  $k$  is the Boltzmann constant,  $\tau^{\alpha}$  is the resolved shear stress on the slip system  $\alpha$ ,  $T$  the absolute temperature,  $\mu$ ,  $\mu_0$  the shear moduli at the current temperature and zero Kelvin (obtained by extrapolation) respectively, and  $Q_0$ ,  $\tau_0$ ,  $p$ ,  $q$  and  $\dot{\gamma}_0$  are material constants.

The slip resistance,  $S$ , and back stress,  $B$ , evolve following coupled hardening laws. Self hardening is assumed and  $S$  and  $B$  are given by,

$$\dot{S}^{\alpha} = [h_S - d_S (S^{\alpha} - S_0^{\alpha})] |\dot{\gamma}^{\alpha}|; \quad \dot{B}^{\alpha} = h_B \dot{\gamma}^{\alpha} - d_B B^{\alpha} |\dot{\gamma}^{\alpha}|. \quad (3)$$

In Eq. (3)  $S_0^{\alpha}$  is the initial slip resistance, which depends on the microstructure (specifically, size and volume fraction of the  $\gamma'$  precipitates) and  $h_S$ ,  $h_B$ ,  $d_S$ ,  $d_B$  are material constants, which depend on microstructure and temperature. The coupling between  $S$  and  $B$  enters through the recovery term  $d_B$  in Eq. (3) which depends explicitly on  $S$  (see [2]). The material constants in Eqs. (2) and (3) have been calculated through a combination of experimental measurements and unit cell studies on representative microstructures, [4], [5]. A typical comparison between the material model and the experimental data at 950°C is shown in Figure 2, which provides the uniaxial tensile response when loaded in the  $\langle 001 \rangle$  direction at different strain rates.

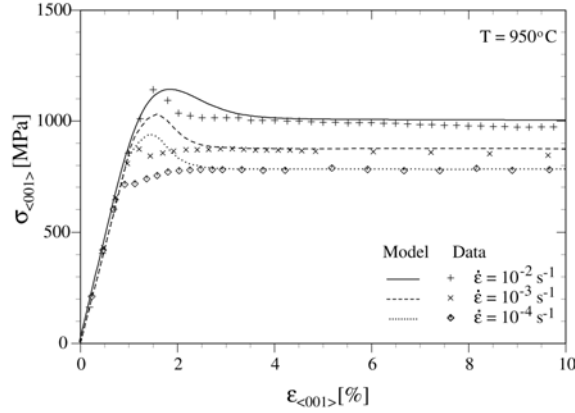


Figure 2: <001> uniaxial response for CMSX4 at three different strain rates—comparison between model and experimental data (from [1]).

### 3 MECHANISTIC MODELLING OF CRACK INITIATION

#### 3.1 Damage Model

In this study, the effect of void growth is accounted for through a damage parameter,  $D$ . Finite element studies of a void embedded within a CMSX4 matrix [2] have determined a critical void volume for crack initiation, which is dependent on stress triaxiality as,

$$\frac{V_c}{V_0} = 1 + b \exp \left[ c \frac{\sigma_m}{\sigma_e} \right], \quad (4)$$

where  $V_0$  is the initial void size,  $b$  and  $c$  are material parameters and  $\sigma_m/\sigma_e$  is the mean (hydrostatic) stress divided by the equivalent stress,  $\sigma_e$ . When coupled with the void growth model for the anisotropic CMSX4 material in [2], a (mesoscopic) failure strain can be determined for crack initiation. It has been shown in [1] that the resultant triaxiality dependent failure strain is relatively insensitive to strain rate and for low triaxialities,  $\sigma_m/\sigma_e < 0.5$ , produces a similar dependence of the (macroscopic) failure strain on triaxiality to that seen for isotropic failure models based on a void coalescence. For convenience, the model can be phrased in terms of a single damage parameter  $D$ , such that at initial loading  $D = 0$  and failure occurs when  $D$  approaches unity, *i.e.*

$$D = \frac{V - V_0}{V_c - V_0}, \quad (5)$$

where  $V$  is the current void volume. When  $D$  reaches unity over a microstructurally significant distance, it can be considered that fracture initiation has occurred. Here the critical distance has been taken to be 50  $\mu\text{m}$ , which is a measure of the initial spacing between voids.

#### 3.2 Explicit void model

The alternative approach adopted is to consider a pre-existing void ahead of the notch, as illustrated in Figure 3. The overall geometry is that of a compact (CT) specimen and the void of

size  $d$  is located a distance  $L$  from the notch root. Thus the growth of the void and the evolution of the local stress triaxiality and inelastic strain due to the void are explicitly accounted for. The mesh used for the damage analysis discussed in the previous section is identical to this one but without the embedded void. For the analysis, the initial void diameter,  $d = 15 \mu\text{m}$ , the notch root radius is  $100 \mu\text{m}$  and the distance from the void to the notch root,  $L$ , is  $150 \mu\text{m}$  (the sensitivity of the result to the void location  $L$  has also been examined). Microcrack initiation occurs when the strain in the vicinity of the void reaches 0.38. This value of failure strain at the meso-scale has been determined from the numerical and experimental studies of [2]. Since a strain gradient exists in the vicinity of the void and the mesh size is finite, it is necessary to specify a critical distance at which the failure strain should be applied. Here the critical distance is taken to be  $1.5 \mu\text{m}$ , which is representative of the size of the  $\gamma'$  precipitates (the predictions are relatively insensitive to this value [6]).

### 3.2 Finite Element Model

A two dimensional FE model of the CT specimen with specimen size  $W = 26 \text{ mm}$  and crack length to specimen width  $a/W = 0.5$  is examined. The smallest element in the mesh is about  $1.5 \mu\text{m}$  and the mesh contains approx. 3,500 elements in total. A four-fold increase in the mesh size has been found to have almost negligible effect on the result. The finite element analyses have been conducted using ABAQUS [7], with a material subroutine to define the CMSX4 response and the damage evolution. Four node, linear plane strain elements have been used and the analysis is fully implicit at the global and local (element) level.

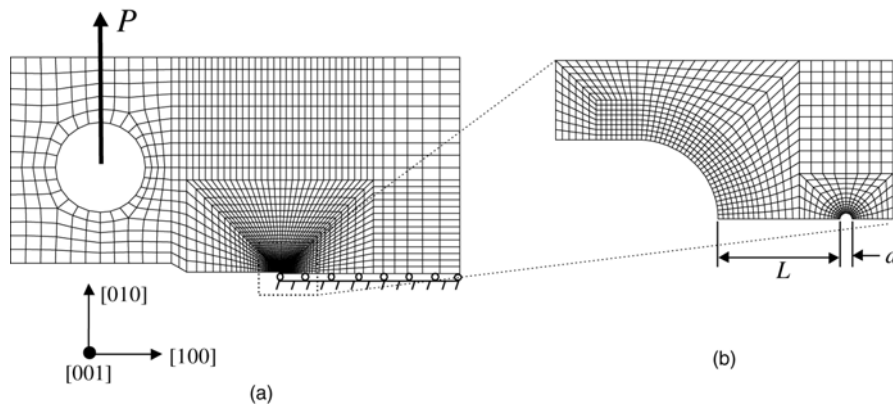


Figure 3: FE mesh for CCG analysis of CT specimen (a) coarse mesh and (b) fine mesh

## 4 FINITE ELEMENT RESULTS

Typical results of the finite element analysis are illustrated in Figure 4. Note that different scales have been used in the two figures in order to highlight the key features. In the analysis the load has been ramped up to a peak value of 4 kN over 400 seconds after which it remains constant. It is seen in Figure 4(a) that the peak damage does not occur directly ahead of the notch plane, but instead at an angle of approx.  $45^\circ$ . Although the triaxiality is highest along the symmetry plane, the peak inelastic strains (in particular the strain on cubic slip systems) are larger in this direction [1]. Thus the damage model predicts that crack growth will not occur perpendicular to the applied load but instead at an angle to the initial notch plane. This result is consistent with fatigue tests on CMSX4 notched bars. Experimental testing is ongoing to confirm this behaviour for the CT specimens under constant (creep) loading.

Figure 4(b) illustrates a typical result for the explicit void analysis. It is expected that at a local level, the result will depend on the void position (distance and angle relative to the notch root). It is observed that the notch and void interact strongly and that the peak strains are found in the vicinity of the void.

Based on the results shown in Fig. 4 the predicted initiation time can be determined using the two methods described in Section 3. Analyses have been carried out for a range of load levels and the results are presented in Figure 5. Two void positions,  $L$ , have been used in the explicit void analysis,  $L/d = 2$  and 10, corresponding to  $L = 30$  and  $150 \mu\text{m}$ , respectively.

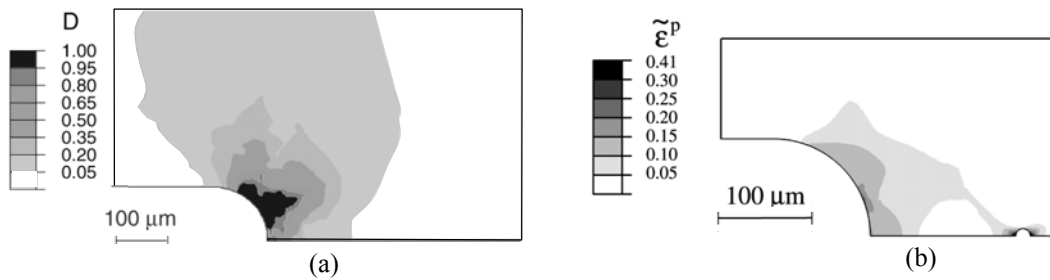


Figure 4: (a) Contours of damage after 1000 hr at 950°C under a 4 kN load. (b) Equivalent inelastic strain for the explicit void analysis, after 400 hours under a 4 kN load. Void spacing,  $L = 150 \mu\text{m}$ .

The strong effect of void location is noted—at a stress intensity factor,  $K = 20 \text{ MPa}\sqrt{\text{m}}$ , the time to crack initiation is approximately an order of magnitude higher when the distance to the notch root is increased by a factor of 5. Since the damage model is accounting for void growth at all points ahead of the notch it is expected to provide an average representation of the explicit void analysis. This is confirmed by the analysis as the result from the damage analysis is found to lie within the two extremes predicted by  $L/d = 2$  and 10 in the explicit void analysis. Note that the critical distance for the damage analysis is  $50 \mu\text{m}$ , which lies within these two limits. It is expected that the predicted initiation times in the damage analysis will depend on the critical distance chosen.

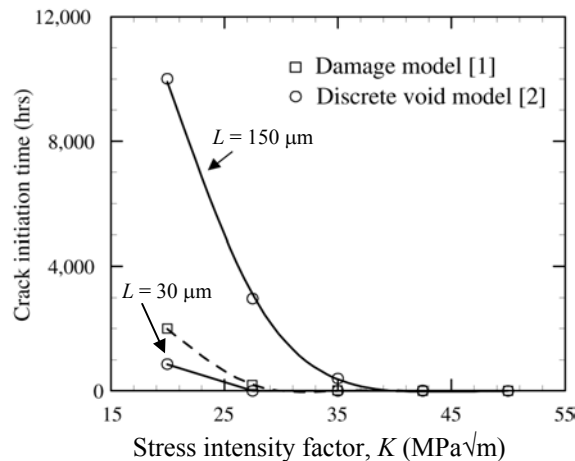


Figure 5: Predicted initiation times using the two models

## 5 DISCUSSION AND CONCLUSIONS

Finite element predictions of crack initiation in a single crystal nickel superalloy have been presented. The results have been found to be sensitive to microstructural features associated with the failure mechanism (e.g. void location). It is expected that the void size will also effect the predicted initiation times. An additional feature, which has been examined in [1] and [3] is the effect of oxidation, which is expected to be active at the temperatures examined here. It is found that for an uncoated alloy exposed to oxygen, the predicted initiation times can be reduced by almost a factor of 2 at the lowest loads (from approx. 10,000 hrs to approx. 600 hrs. for CMSX4 at 950°C). Experimental analyses are ongoing to confirm these predictions and to provide a robust mechanistic-based model to predict crack growth in nickel superalloys over the range of operating conditions.

## 6 REFERENCES

- [1] Dumoulin, S., Busso, E.P. and O'Dowd, N.P. "A multiscale approach for coupled phenomena in FCC materials at high temperatures", *Philosophical Magazine*, **83** 3895–3916, 2003,
- [2] Dennis, R. J., Mechanistic modelling of deformation and void growth behaviour in superalloy single crystals, PhD thesis, Imperial College London, 2000.
- [3] Busso, E.P. and McClintock, F.A., "A dislocation mechanics-based crystallographic model of a B2-type intermetallic alloy", *International Journal of Plasticity*, **12**, 1–28, 1996..
- [4] Busso, E.P., Meissonnier, F. and O'Dowd, N.P., "Gradient-dependent deformation of two-phase single crystals, *Journal of the Mechanics and Physics of Solids*", **48**, 2333–2361, 2000.
- [5] Meissonnier, F., Busso, E.P. and O'Dowd, N.P., "Finite element implementation of a generalised non-local rate dependent crystallographic formulation for finite strains, *International Journal of Plasticity*", **17**, 601– 640, 2001
- [6] Zhao, L.G., O'Dowd, N.P. and Busso, E.P. "A Coupled Approach to the Study of High Temperature Crack Initiation in Single Crystal Nickel-Base Superalloys", work in preparation, 2004
- [7] ABAQUS version 5.8. Hibbitt, Karlsson & Sorensen, Inc., 1998.
- [8] Boubidi, P., "Experimental characterization and numerical modelling of low cycle fatigue in a nickel base single crystal superalloy under multiaxial loading" PhD Thesis, Centre des Materiaux, Ecole des Mines de Paris, France, Dec. 2000.